

Review

Open Access



A versatile messenger for chirality communication: asymmetric silica framework

Xinling Liu^{1,*}, Ren-Hua Jin^{2,*}

¹The Education Ministry Key Lab of Resource Chemistry, College of Chemistry and Materials Science, Shanghai Normal University, Shanghai 200234, China.

²Department of Material and Life Chemistry, Kanagawa University, Yokohama 221-8686, Japan.

***Correspondence to:** Prof. Xinling Liu, The Education Ministry Key Lab of Resource Chemistry, College of Chemistry and Materials Science, No.100 Guilin Rd, Shanghai Normal University, Shanghai 200234, China. E-mail: xliu@shnu.edu.cn; Prof. Ren-Hua Jin, Department of Material and Life Chemistry, Kanagawa University, 3-27-1 Rokkakubashi, Kanagawa-ku, Yokohama-shi, Yokohama 221-8686, Japan. E-mail: rhjin@kanagawa-u.ac.jp

How to cite this article: Liu X, Jin RH. A versatile messenger for chirality communication: asymmetric silica framework. *Chem Synth* 2021;1:14. <https://dx.doi.org/10.20517/cs.2021.16>

Received: 29 Oct 2021 **First Decision:** 23 Nov 2021 **Revised:** 3 Dec 2021 **Accepted:** 7 Dec 2021 **Published:** 17 Dec 2021

Academic Editor: Bao-Lian Su **Copy Editor:** Xi-Jun Chen **Production Editor:** Xi-Jun Chen

Abstract

Asymmetric tetrahedral carbon is the basic structural unit of many organic compounds in life and its molecular chirality plays a key role in regulating biological functions. Silica (SiO₂) is highly earth abundant and its basic unit is also the tetrahedral form of SiO₄. However, much less attention has been paid to the molecular-scale chirality of SiO₂ frameworks with repeating SiO₄ units because it is challenging to enantioselectively control the molecular structures of SiO₂. Research into the chiral molecular structures of SiO₂ deserves to be a significant topic for understanding widespread chiral phenomena and for exploring the chiral properties hidden in inorganic matter. This review highlights the asymmetric synthesis strategies that endow SiO₂ with chirality transferred from asymmetric carbon at the molecular scale. The chirality transfer ability of SiO₂ is also demonstrated for the construction of various inorganic and/or organic chiral materials with a wide range of applications in asymmetric synthesis, circularly polarized luminescence and Raman scattering-based chiral recognition.

Keywords: Chiral silica, asymmetric SiO₄ tetrahedra, chirality transfer, circularly polarized luminescence, enantioselective Raman scattering



© The Author(s) 2021. **Open Access** This article is licensed under a Creative Commons Attribution 4.0 International License (<https://creativecommons.org/licenses/by/4.0/>), which permits unrestricted use, sharing, adaptation, distribution and reproduction in any medium or format, for any purpose, even commercially, as long as you give appropriate credit to the original author(s) and the source, provide a link to the Creative Commons license, and indicate if changes were made.



INTRODUCTION

Chirality divides matter or light into a pair of non-superimposable enantiomeric forms with a mirror image relationship and occurs on a broad length scale from the molecular, to the nano/micro and even cosmic levels. In particular, the significance of molecular-scale chirality has been broadly accepted since 1848, when Louis Pasteur linked optical activity with the stereostructures of molecules after resolving the structure of sodium ammonium (\pm)-tartrate crystals under a light microscope^[1]. It is known that proteins consisting of amino acid residues are chiral on all primary, secondary, tertiary and quaternary structural levels, among which the primary molecular chirality of amino acids plays a key role in chiral features and biological functions at higher levels^[2]. Therefore, the chirality of synthesized molecules or materials is a property of concern, especially when they are associated with living organisms or chiral light. In this context, chiral inorganic materials have received ever-increasing attention over the past two decades, despite the fact that inorganic materials are often considered as being achiral^[3-6].

As an important and enormous class of inorganic material, silica (SiO_2) is highly abundant and widely used in many industries and research fields. Studies of the chirality of SiO_2 date back to 1812 when Jean-Baptiste Biot found that natural quartz (crystalline SiO_2) is able to rotate the plane of polarized light, which is an optical manifestation of chirality^[7]. However, the chirality of SiO_2 was not fully appreciated until the end of the 20th century. Since 2000, a variety of chiral SiO_2 nanomaterials have been reported^[8-18], which find many applications in chiral separation, biomedical therapy and asymmetric catalysis^[19-22]. With modern spectroscopic and electron microscopy techniques, the chiral features of such SiO_2 materials have been demonstrated by: (1) helical outward shapes with pitches of over tens of nm (typical examples shown in [Figure 1A-C](#)), which are duplicated from the helical structures of organic templates in the sol-gel synthesis processes; and (2) inward chiral cavities, which are imprinted by chiral small molecules [[Figure 1D](#)]. Unfortunately, the chiral structures of SiO_2 close to the molecular scale (on the Si-O-Si skeleton) have been underexplored, in spite of the long history (over two centuries) of SiO_2 chemistry and the aforementioned significant progress in artificial chiral SiO_2 .

To probe the chirality of SiO_2 near the molecular scale, the molecular structures of SiO_2 must be considered. The basic unit of SiO_2 is the SiO_4 tetrahedra, which are interconnected by -Si-O-Si- bonds to form a three-dimensional (3D) structure. Consequently, SiO_2 is a kind of polymer that uses SiO_4 tetrahedra as monomer units. Although it is often assumed that the SiO_4 units are regular tetrahedra (i.e., the lengths of the four Si-O bonds are the same), both the lengths of the Si-O bonds and the -O-Si-O- angles are in fact variable [[Figure 2A](#)], which influences the arrangements and orientations of SiO_4 tetrahedra in 3D space^[23]. For example, the SiO_4 tetrahedra in L-form quartz arrange into a chiral pattern of a left-handed helix (with helical pitches of less than 1 nm) along the c axis, while a right-handed one exists in R-form quartz [[Figure 2B](#)]^[24]. It is noteworthy that the SiO_4 unit in quartz is not a regular tetrahedral group and the formation of such helices is a result of energy minimization among these irregular SiO_4 units. According to the previous characterization results of quartz samples, the SiO_4 unit is not a perfect tetrahedron as there are two pairs of bonds with different lengths (1.608 and 1.609 Å), two angles of 110.5°, two angles of 108.7°, one angle of 109.5° and one angle of 108.8°^[25,26].

In addition to quartz, chiral distorted AB_4 (A = Si; B = O, Si or Al) structures are common in many natural and synthetic silicate zeolites^[27]. In quartz and zeolites, even if the deviation of the elementary SiO_4 unit from a regular tetrahedron is small, the distortion will become amplified in larger tetrahedral units, such as SiSi_4 [i.e., Si-(O-Si)₄ without oxygen atoms]. Consequently, the distortion of AB_4 units plays a significant role in the chirality of SiO_2 and zeolite frameworks, and experimentally it was confirmed that these chiral zeolites are capable of the enantioselective absorption of amino acid enantiomers. Moreover, based on the

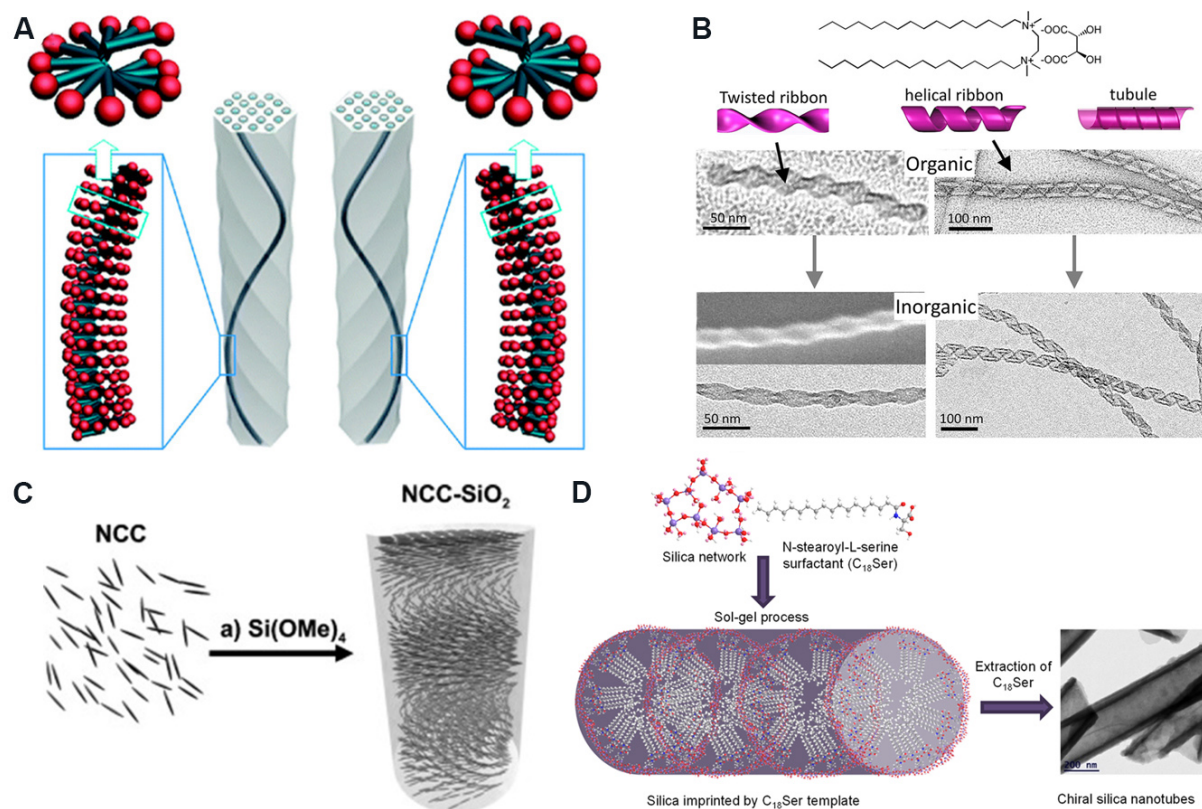


Figure 1. Typical synthesized chiral SiO_2 nanomaterials. (A) Schematic models for left- (left) and right-handed (right) chiral mesoporous silica derived from the helical propellerlike packing of chiral amphiphilic molecules. This figure is used with permission from the American Chemical Society^[10]. (B) TEM images of self-assemblies of amphiphilic surfactants of 16-2-16 and their transcription into twisted and helical SiO_2 . This figure is used with permission from the American Chemical Society^[13]. (C) A schematic model for chiral nematic mesoporous SiO_2 films templated from the nematic ordering of nanocrystalline cellulose (NCC). This figure is used with permission from John Wiley and Sons^[14]. (D) Imprinted chiral SiO_2 nanotubes synthesized using a chiral N-stearoyl L-serine (C_{18}Ser) anionic surfactant template. This figure is used with permission from the American Chemical Society^[16].

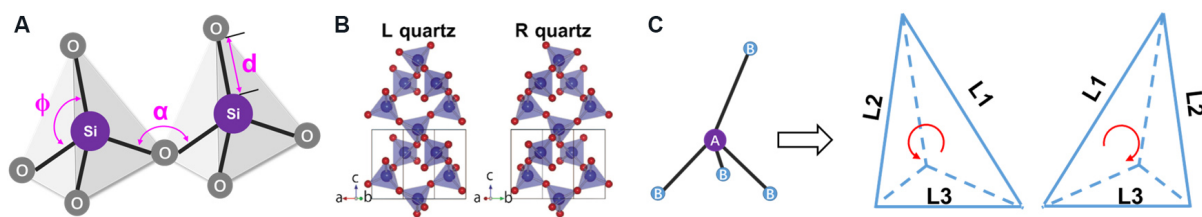


Figure 2. (A) Basic SiO_4 tetrahedra in SiO_2 framework [angles (α , ϕ) and bond lengths d are variable]. (B) Crystal structures of L- and R-quartz. This figure is used with permission from the American Physical Society^[24]. (C) Schematic models of a pair of AB_4 tetrahedral enantiomers with clockwise or counter-clockwise patterns.

variety of bond lengths and angles in AB_4 structures, Yogeve-Einot *et al.*^[26] proposed chirality assignment rules for AB_4 tetrahedral enantiomers [Figure 2C]. Firstly, the perimeter length of the four triangle faces of the B_4 pyramid is calculated. Secondly, the triangle with the largest perimeter is placed in the plane of the page and the fourth substituent behind the page. Finally, a right-handed AB_4 tetrahedron is assigned if the direction from the longest edge (L1) to the shortest one (L3) in the plane of the page is clockwise, whereas a left-handed tetrahedron is assigned for a counterclockwise direction. In spite of the concepts proposed above and some simulation models of chiral Si centers^[28], it is not straightforward to detect the chirality of

SiO₂ down to the molecular level, possibly due to the racemic state where two SiO₄ tetrahedral enantiomers co-exist in equal amounts. Moreover, it is still difficult to design and confirm molecular-scale chirality for synthesized SiO₂ from an experimental perspective.

Traditionally, SiO₂ is formed in solutions using a sol-gel process with controllable structures and morphologies of SiO₂ gel on a relatively high length scale (over 10 nm). In contrast, in many biosilicification processes in diatoms and sponges, bio-SiO₂ is usually deposited on the solid surfaces of many biomolecular templates, where the formation of SiO₂ sol (less than 10 nm) is well directed by organic templates due to organic-inorganic interactions^[29,30]. Since the sizes of SiO₂ sol are closer to the molecular scale than SiO₂ gel, it is possible to endow SiO₂ with molecular-scale chirality if chirality communication occurs between SiO₂ sol and suitable chiral sources in the early stage of the sol-gel process. Since 2004, we have reported the use of a bioinspired method to construct SiO₂ nanofibers using crystalline assemblies of linear polyethyleneimine (PEI) as catalytic templates^[31-33]. This method is also a solid-state template-assisted process, where SiO₂ is site-selectively produced on PEI surfaces but rarely in the solution. Furthermore, when PEI is complexed with chiral sugar acids (e.g., tartaric and glucaric acids), the as-formed crystalline aggregates with a pair of -HNH...OC=O are still effective in prompting silicification, accompanied by chirality transfer from organic templates to SiO₂^[34,35]. Surprisingly, even after removing the organic templates, the as-obtained SiO₂ displays unique chiral properties associated with their asymmetric siliceous molecular structures, which are corroborated by many experimental results, as shown below. Therefore, such chiral SiO₂ structures offer us a good platform to understand the molecular-scale chirality of SiO₂.

This mini-review focuses on recent research into these chiral SiO₂ nanofibers. We firstly show the preparation procedures of SiO₂ and provide spectroscopic evidence of their chirality, which is further supported by the power of SiO₂ to transfer chirality information to other inorganic nanoparticles (NPs) and organic polymers. In the subsequent sections, the potential of SiO₂ in manipulating chiral light emissions [circularly polarized luminescence (CPL)] and achiral light scattering (enantioselective Raman scattering for chiral recognition) is discussed. Finally, a short conclusion and perspectives are given.

CHIRAL SiO₂ NANOFIBERS WITH ASYMMETRIC SiO₄-BASED POLYMERIC NETWORKS

The typical preparation route using tartaric acids (tart) for chiral SiO₂ nanofibers is described in [Figure 3A](#). The crystalline complexes composed of PEI and tart are prepared by dissolving the PEI and tart in hot water, followed by a cooling-induced crystallization process. After the addition of tetramethoxysilane (TMOS) into the PEI/tart dispersion in water, the hydrolysis and polycondensation of TMOS into SiO₂ around the PEI/tart templates rapidly finishes, resulting in PEI/tart@SiO₂ hybrids. SiO₂ nanofibers are obtained by removing the PEI and tart after calcination at a high temperature (500-900 °C) in air. The handedness tags (D-, L- and DL-) of PEI/tart, PEI/tart@SiO₂ and SiO₂ are consistent with those of the tart used. As shown by scanning electron microscopy (SEM) images, the morphologies of the PEI/tart templates are kept on PEI/tart@SiO₂ [[Figure 3B](#) and [C](#)] and both D-PEI/tart@SiO₂ and L-PEI/tart@SiO₂ appear as nanofibers in the high-magnification SEM images [[Figure 3D](#) and [E](#)]. Unlike most helical SiO₂ nanomaterials, it is difficult to observe chiral features on the exterior of SiO₂ nanofibers based on electron microscopy.

The chiroptical activity of calcinated SiO₂ has been examined by electronic circular dichroism spectroscopy. Corresponding to the characteristic absorption bands of SiO₂ (from 185 to 195 nm), the negative circular dichroism (CD) signal of D-SiO₂ is a mirror image of the positive one of L-SiO₂, while DL-SiO₂ is CD silent [[Figure 3F](#)]^[34]. In addition, when some achiral chromophores [e.g., tetrakis(3,5-hydroxyphenyl)porphyrin] are physically absorbed onto SiO₂, they show antipodal inductive CD signals on D-SiO₂ and L-SiO₂ but

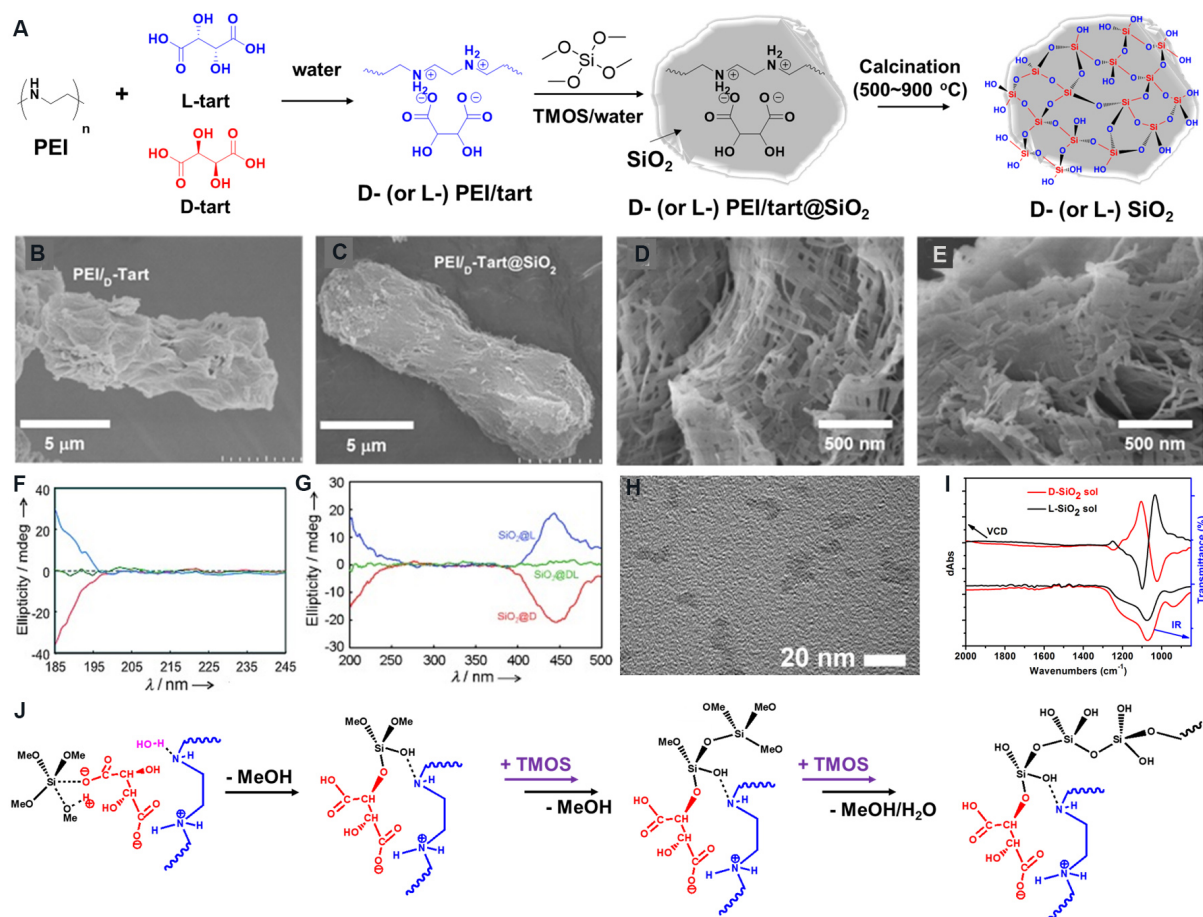


Figure 3. (A) Schematic showing the synthesis of chiral SiO₂ nanofibers using PEI/tart templates. (B, C) SEM images of (B) D-PEI/tart and (C) D-PEI/tart@SiO₂. (D, E) High-magnification SEM images of (D) D-PEI/tart@SiO₂ and (E) L-PEI/tart@SiO₂. (F) CD spectra of D-, L- and DL-SiO₂. (G) CD spectra of D-, L- and DL-SiO₂ absorbed with tetrakis(3,5-hydroxyphenyl)porphyrin. This figure is used with permission from John Wiley and Sons^[34]. (H) TEM image of D-SiO₂ sol derived from D-SiO₂ nanofibers: (I) VCD (left) and IR (right) spectra of D-SiO₂ and L-SiO₂ sol. This figure is used with permission from the Royal Society of Chemistry^[36]. (J) A schematic proposal for the formation of chiral SiO₂ on PEI/tart templates. PEI: Polyethyleneimine; SEM: scanning electron microscopy; CD: circular dichroism; VCD: vibrational circular dichroism.

remain CD inactive on DL-SiO₂ [Figure 3G]. Furthermore, long SiO₂ nanofiber bundles can be crushed into SiO₂ NPs (SiO₂ sol) with an average size of ~7 nm by hydrothermal treatment [Figure 3H]^[36]. According to vibrational circular dichroism (VCD) spectroscopic analysis, D-SiO₂ and L-SiO₂ sols show opposite Cotton VCD signals (within 1000-1200 cm⁻¹) corresponding to the stretching vibrations of Si-O-Si bonds [Figure 3I], implying the existence of twisted structures between asymmetric Si centers. Moreover, achiral molecules physically absorbed onto SiO₂ sol also display inductive VCD signals. Consequently, the CD and VCD signals above are in favor of the molecular-scale chirality existing on SiO₂ nanofibers. Additional related proof is provided in the following sections using SiO₂ as a chirality source to construct a series of chiral nanomaterials.

Nevertheless, it is difficult to clarify the chirality transfer mechanism from PEI/tart to SiO₂ due to a lack of effective analysis protocols. As confirmed in previous reports, charged pairs consisting of amines and carboxylic acids are efficient to accelerate the transformation of alkoxysilanes into SiO₂^[37]. Based on nuclear magnetic resonance (NMR), X-ray diffraction and elemental analysis of the crystalline PEI/tart aggregates formed in water, the molar ratio of NH/COOH/H₂O is estimated as 1:1:1^[34]. Thus, the crystalline surface is

densely covered by many $\text{-HNH}\cdots\text{OC=O}$ pairs, which act as catalytic sites for the silicification of TMOS. We proposed previously a tentative chirality transfer scenario from PEI/tart to the resulting silica^[38], as shown in [Figure 3J](#). The carboxylate group in the $\text{-HNH}\cdots\text{OC=O}$ pair nucleophilically attacks the Si of TMOS to give a pentacoordinated structure and a silane moiety bonded by the secondary alkoxy group of tartrate is then generated and anchored on PEI/tart with the removal of the methoxy group. Subsequently, the group of Si-OH on the silane moiety is activated by -NH- and reacts further with other TMOS molecules, resulting in the formation of an -O-Si-O- network. Such a reaction occurs simultaneously here and there around whole the surface of PEI/tart. Because the initial anchor moiety is located in the chiral domain of PEI/tart, the lengths of the Si-O bonds and the angles of the O-Si-O bonds will be influenced by the chiral spatial structures of PEI/tart and the following polymerization and cyclization can be regulated through enantiomeric enrichment to generate asymmetric polysilicate structures. With an increasing amount of SiO_2 shell, the PEI/tart templates become covered by SiO_2 and their chiral influences are weakened. However, the early formed SiO_2 layer can be used as a chiral seed to maintain the following SiO_2 deposition through epitaxial growth with self-amplification of the chirality. In brief, these three steps (anchoring, polymerization and epitaxial growth) are key for the generation of chiral structures on SiO_2 .

CHIRALITY TRANSFER FROM SiO_2 TO INORGANIC NANOMATERIALS

It has been confirmed that molecules or NPs, which are either physically attached to or chemically formed in chiral SiO_2 nanomaterials, can become chiroptically active in CD spectra. However, the as-observed optical activity is a result of induced CD and does not mean structural chirality. For example, silver NPs *in-situ* formed in helical mesoporous SiO_2 are CD active but return to being CD inactive after removing the SiO_2 host, suggesting that chirality transfer is inefficient from helical SiO_2 to metal NPs^[39]. It is reasonable to propose that the chirality in many previously reported chiral SiO_2 materials disappears when their outward helical morphologies or inward chiral cavities are destroyed^[40].

In contrast, chiral SiO_2 nanofibers with sturdy chiral structures close to the molecular scale possess an excellent ability of chirality transfer. For example, Au NPs were firstly *in-situ* synthesized on chiral SiO_2 nanofibers via thermal reduction at high temperatures (500-800 °C)^[41]. Surprisingly, after dissolving SiO_2 nanofibers by hydrothermal treatment or etching using NaOH solutions, the as-isolated Au NPs [[Figure 4A](#) and [B](#)] remain CD active and are able to make other achiral molecules to present inductive CD signals. Compared with common Au NPs, the lattices of chiral Au NPs are distorted, as shown by scanning transmission electron microscopy (STEM) images [[Figure 4C](#) and [D](#)], which is indicative of the intrinsic structural chirality of Au NPs at the atomic scale. Based on Raman spectra, the chirality of the Au NPs is proven by their enantioselective recognition toward chiral small molecules. In another study by Wei *et al.*^[42], wavelike lattices [[Figure 4E](#) and [F](#)] are also found on Ag nanohelices (NHs) prepared by glancing angle deposition and these chiral lattices can affect the orientation of molecules to achieve enantioselective synthesis with enantiomeric excess up to 5%.

In organic chemistry, chiral pool synthesis is straightforward and can be used to prepare optically active products that are transformed from chiral starting materials. The basic unit in crystalline Si is also a regular SiSi_4 tetrahedron with one central Si atom connected to four Si atoms at the corners. Due to the high symmetry of crystal structures, it is difficult to produce chiral Si. However, asymmetric SiO_4 tetrahedra may be used as chiral pools to generate asymmetrically distorted SiSi_4 tetrahedra. On this basis, via a solid-state magnesiothermic reaction at 500-600 °C, chiral SiO_2 nanofibers (with an average diameter of ~10 nm) were reduced by magnesium and transformed into Si nanoplates of several hundreds of nm in size [[Figure 5A](#) and [B](#)]^[36]. Despite the morphological change, the chiroptical activity of Si is confirmed in their CD and UV-Vis absorption spectra [[Figure 5C](#) and [D](#)]. Moreover, achiral molecules physically absorbed on these Si

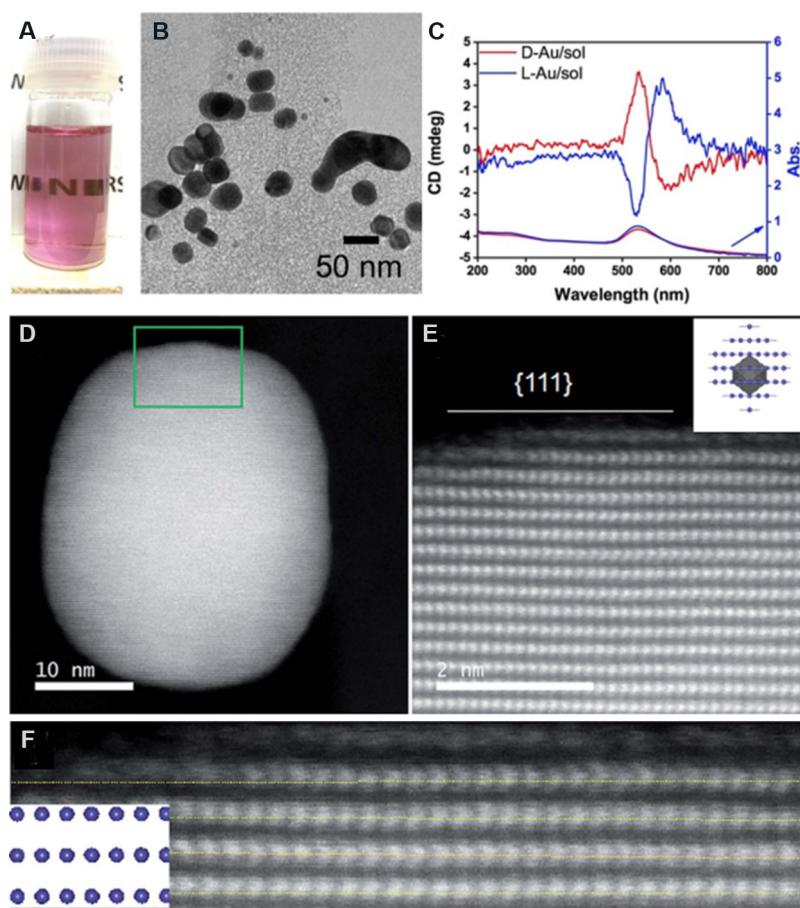


Figure 4. (A) Photograph of aqueous solution of L-Au NPs after hydrothermal treatment of L-Au@SiO₂. (B) TEM image of L-Au NPs. (C) CD and UV/Vis spectra of D-Au and L-Au NPs. (D) Low magnification STEM image (viewed along the direction of {111}) of D-Au@SiO₂-500. (E) Atomic resolution STEM image of the square region in (D). (F) Enlarged image of (E) showing the non-straight arrangement of the atomic array. This figure is used with permission from the Royal Society of Chemistry^[41]. NPs: Nanoparticles; TEM: transmission electron microscopy; CD: circular dichroism; STEM: scanning transmission electron microscopy.

nanoplates show induced VCD signals. This provides a special self-directed chirality transfer mechanism from amorphous silica to crystalline silicon. These two examples indicate that SiO₂ nanofibers can impart inherent chiral structures to products *in-situ* synthesized on the surfaces of SiO₂.

CHIRALITY TRANSFER FROM SiO₂ TO ORGANIC POLYMERS

Synthesis of chiroptically active cross-linked polymers

Polymers with chiroptical activity are widely used for various purposes, including chiral discrimination, sensing and optical devices. Usually, the chirality of polymers is controlled using chiral organic substances (e.g., monomers, catalysts and auxiliaries). However, from the perspective of the origins of life, there are arguments that inorganic minerals enrich monomer precursors and then direct their polymerization into larger chiral biological polymers during the formation of early cells^[43,44]. Therefore, research on the chirality transfer from inorganics to organics is a vitally important topic. With the above success in the induced chirality of small inorganic NPs by chiral SiO₂ nanofibers, the feasibility of the chiral synthesis of polymers on SiO₂ surfaces is also demonstrated below.

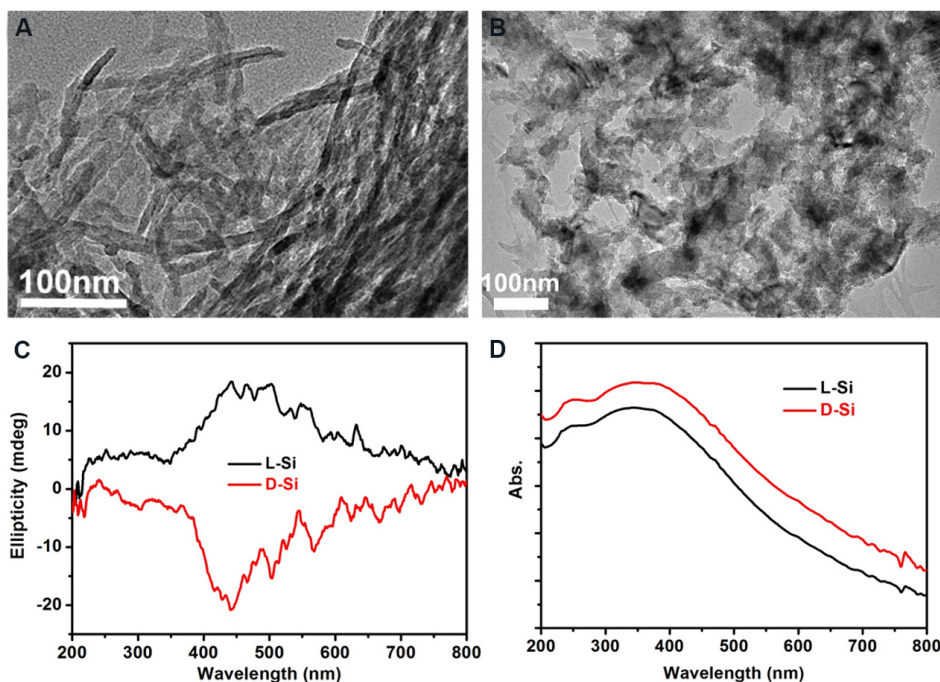


Figure 5. TEM images of (A) D-SiO₂ and (B) D-Si. (C) CD (left) and (D) UV/Vis absorption (right) spectra of D- and L-Si. This figure is used with permission from the Royal Society of Chemistry^[36]. CD: Circular dichroism.

The first example is the synthesis of phenolic resin (RF) using achiral monomers of resorcinol (R) and formaldehyde (F). At first, the polymerization of R and F was conducted using PEI/tart@SiO₂ as the chiral template^[45]. Although the as-obtained RF shows obvious CD signals, it is difficult to judge whether the chiroptical activity of RF is induced by chiral tart or chiral SiO₂. The tart in PEI/tart@SiO₂ were removed via treatment of the as-prepared sample using HCl (aq), with only PEI left in the SiO₂ nanofibers^[46]. Because the polymerization of R and F can take place under a basic catalyst, the basic amine groups on PEI act as catalysts to initiate the polymerization. Indeed, RF is successfully deposited on SiO₂ nanofibers and shows chiroptically activity in the CD spectra.

Not limited to PEI, other amine group-bearing surface modifiers have also proven to be effective. In a recent study, the powders of PEI/tart@SiO₂ were firstly treated under high temperature (600 °C) in air to remove the organic species of PEI and tart. As shown in Figure 6A, four types of silane coupling agents (SCAs) were selected, namely, 3-(trimethoxysilyl)propylamine (with a primary amino group of NH₂-, 1°P), N-methyl-3-(trimethoxysilyl)propylamine (secondary NHMe-, 2°P), N,N-dimethyl-3-(trimethoxysilyl)propylamine (tertiary NMe₂-, 3°P) and N-(3-triethoxysilylpropyl)-4,5-dihydroimidazole (with an imidazole group, Im)^[47]. These SCAs were used as surface modifiers to prepare amine-modified chiral SiO₂ (i.e., 1°P-SiO₂, 2°P-SiO₂, 3°P-SiO₂ and Im-SiO₂). Due to the base nature of SCAs, the polymerization of R and F occurs site selectively on the surface of SiO₂ nanofibers when heating at 60 °C. All these four kinds of SCAs can induce the formation of RF based on NMR analysis. For example, the tertiary amino-modified SiO₂ (3°P-SiO₂) possesses the lowest nitrogen content but shows the highest yield of RF, with a mass ratio of 51.5 (SiO₂):40.3 (RF):8.2(SCA) in the 3°P-SiO₂@RF composites. Although these amino residues are not chiral, the inductive CD signals with mirror image relationships are observed in the absorption range of each amino residue chemically anchored on D- and L-form SiO₂, implying the chirality penetration from SiO₂ to amino residues. The chirality information is further permeated to RF resins, with a pair of opposite CD signals in D- and L-form 3°P-SiO₂@RF appearing in the range between 300 and 800 nm [Figure 6B], which

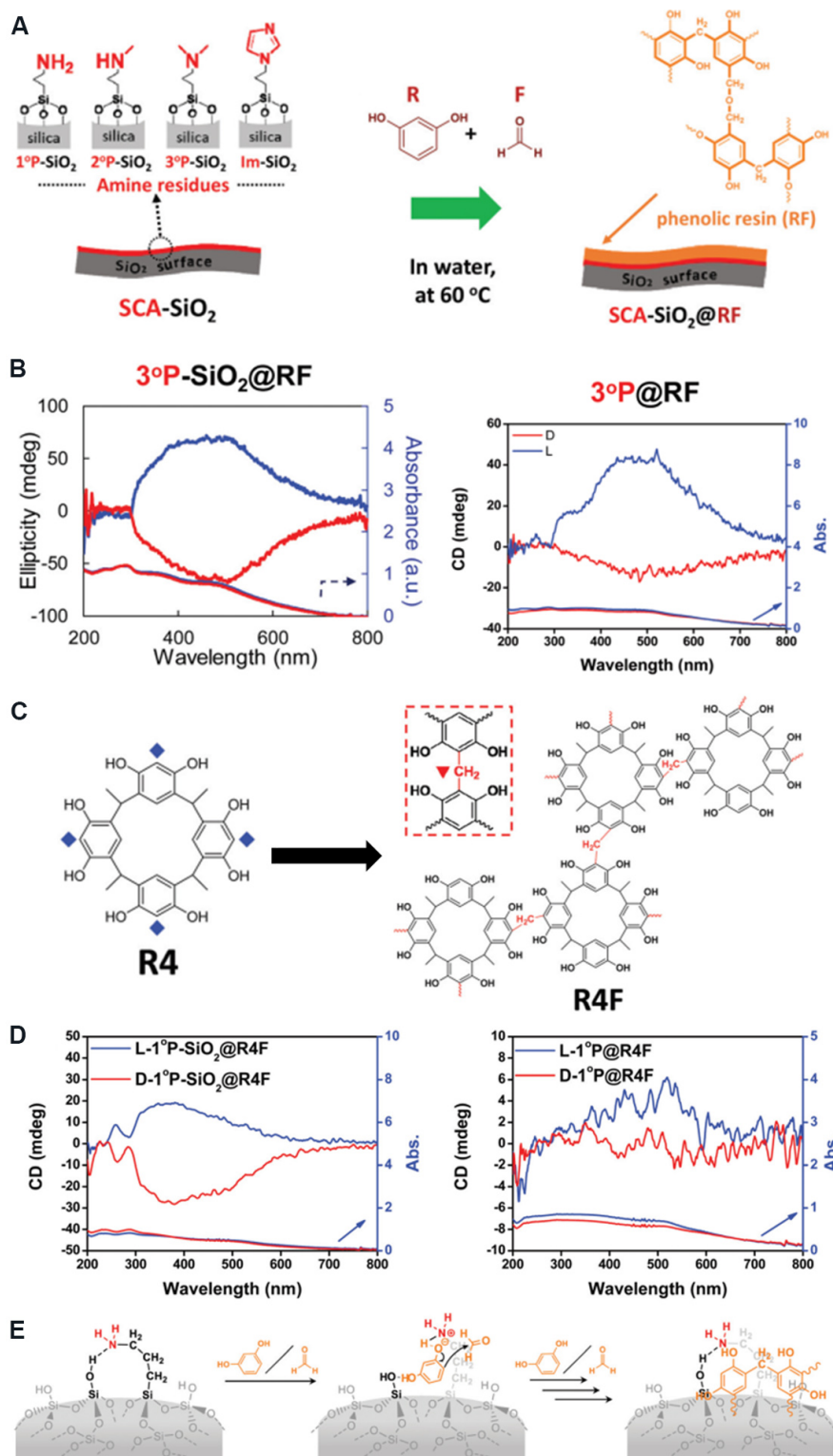


Figure 6. (A) Synthesis of RF resin on SCA-modified chiral SiO_2 , (B) CD and UV-Vis absorption spectra of $3^\circ\text{P-SiO}_2\text{@RF}$ (left) and 3°P@RF (right). (C) Molecular structures of R4 and R4F. (D) CD and UV-Vis absorption spectra of $1^\circ\text{P-SiO}_2\text{@R4F}$ (left) and 1°P@R4F (right). (E) A proposed polycondensation reaction of R with F on the chiral SiO_2 surface chemically bonded with amine residues. This figure is used with permission from the Royal Society of Chemistry^[47]. SCA: Silane coupling agent; CD: circular dichroism; R: resorcinol; F: formaldehyde.

are attributed to the π -electron conjugation and π - π interaction of RF. Similar to the cases of chiral Au NPs and Si nanoplates, the isolated RF still maintains its chiroptical activity even after the removal of SiO₂ using a hydrogen fluoride solution [Figure 6B], indicating that the inherent chirality is steadily endowed on RF.

Furthermore, through the condensation reaction between resorcinol and acetaldehyde, resorcinol was transformed into achiral resorcinarene (R4). After the absorption of R4 onto 1°P-SiO₂ (1°P-SiO₂@R4), a resorcinarene (R4)-based phenolic resin (R4F) is synthesized by the cross-linking between the aromatic rings of R4 with the addition of formaldehyde [Figure 6C]. The D- and L-1°P-SiO₂@R4F also exhibited antipodal CD signals between 250 and 700 nm [Figure 6D]. These CD signals are still found on R4F peeled from SiO₂ [Figure 6D], although the CD signals became weaker compared with those of 1°P-SiO₂@R4F. The chiral discrimination ability of R4F toward racemic mandelic acid was revealed by CD spectroscopy, with D-1°P-SiO₂@R4F favoring the adsorption of D-MA while L-1°P-SiO₂@R4F preferred L-MA.

Because no chiral carbon centers exist in the molecular structures of R, R4 and F, the origin of chirality in RF and R4F may be associated with their cyclic residues in the network backbone. It is possible that the cyclic residues resembling calixarene derivatives are deformed with the non-equivalent substitution in the periphery of the cyclic residues to generate axial asymmetry. A mechanism is proposed [Figure 6E] where the amine residues can interact with the chiral sites of Si*-OH via hydrogen bonds to form loop-like domains with potential chirality, which facilitates the chiral transfer to resorcinol and the following intermediates, thus regulating the polymer growth and inducing the axial asymmetry of cyclic residues.

It seems that cross-linked polymers can be endowed with chiroptical activity on these SiO₂ nanofibers. To further support this point, other two kinds of polymers are synthesized via the radical polymerization of achiral divinylbenzene (DVB) or N,N'-methylenebisacrylamide (MBA) around SiO₂ [Figure 7A]^[48]. The tart in PEI/tart@SiO₂ was firstly removed by HCl to obtain PEI/SiO₂. Because PEI can easily react with many organics, including alkyl halide, 4,4'-bis(chloromethyl)biphenyl (Bp) was chemically bonded onto the PEI fraction to obtain biphenyl group-bearing SiO₂ (Bp-PEI/SiO₂). On this basis, the hydrophilic surfaces of SiO₂ become hydrophobic and absorb the DVB (or MBA) monomers. The polymer of polydivinylbenzene (PDVB) is synthesized in the presence of azo-initiators when heating at 80 °C, as confirmed by NMR analysis [Figure 7B]. In the composites of PDVB-hybridized chiral silica (PDVB@Bp-PEI/SiO₂), the mass ratio of PDVB is ~32.1%. After removing SiO₂ using 5 wt.% NaOH (aq), the liberated PDVB showed a pair of opposite CD signals in its absorption band (250-350 nm, Figure 7C). When MBA is used as the precursor, the as-prepared polymers of poly(N,N'-methylenebisacrylamide) (PMBA) also show CD signals in their absorption bands at ~290 nm. Furthermore, the chirality of PDVB and PMBA is confirmed using an achiral porphyrin derivative of tetrakis(4-carboxyphenyl)porphyrin (TCPP) as the probe molecule. By mixing TCPP with PDVB (or PMBA), the inductive CD Cotton signals of TCPP with mirror relationships are present around the characteristic absorbance at the Soret and Q-bands of TCPP [Figure 7D]. Consequently, it can be concluded that these chiral SiO₂ nanofibers are powerful in the asymmetric synthesis of chiroptically active cross-linked polymers through the rational design of surface modifiers, catalysts and monomers.

Enantioselective control of polymer crystallization

SiO₂ nanofibers affect not only the polymerization but also the crystallization process of polymers. For example, due to the periodic helical twist of lamellar, the crystalline polymer of poly(ϵ -caprolactone) (PCL) can form banded spherulites when blended with poly(vinylbutyral) (PVB), where both right- and left-handed twists of PCL lamellae are produced randomly. When SiO₂ nanofibers are employed as nucleating agents to mediate the crystallization of PCL/PVB blends, it is found that SiO₂ can accelerate the nucleation

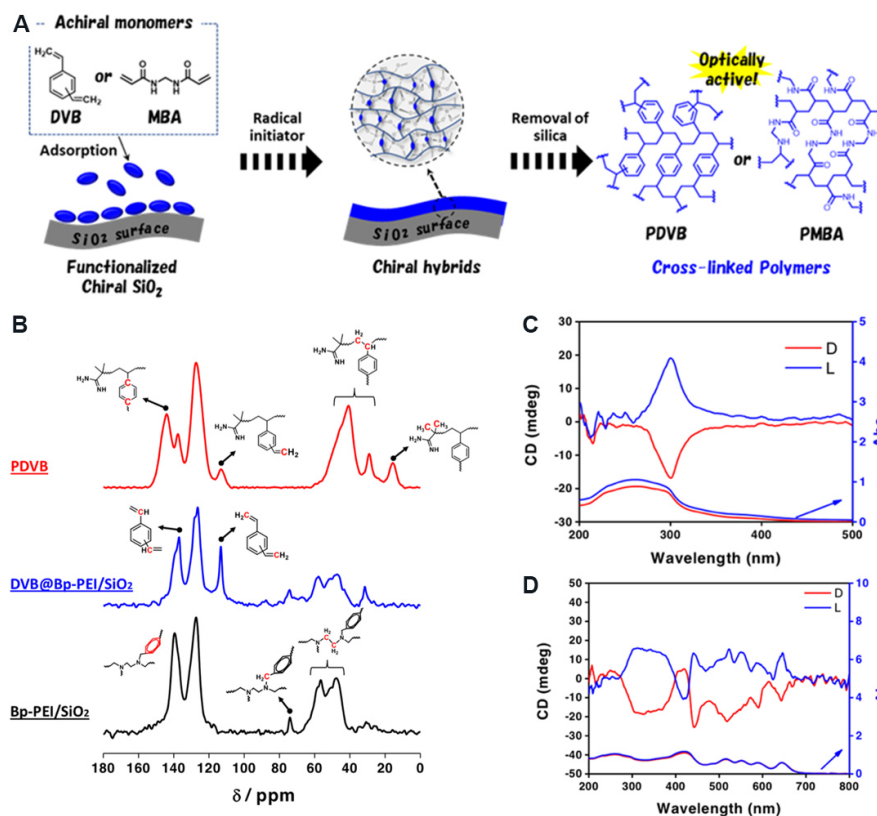


Figure 7. (A) Synthesis of chiral cross-linked polymers of PDVB and PMBA via radical polymerization of divinyl monomers around biphenyl group-bearing SiO_2 nanofibers. (B) ^{13}C NMR spectra of L-form Bp- SiO_2 , DVB@Bp-PEI@ SiO_2 and isolated PDVB. Solid-state CD and UV-vis absorption spectra of (C) chiral isolated PDVB and (D) TCP@PDVB. This figure is used with permission from John Wiley and Sons^[48]. DVB: Divinylbenzene; MBV: N,N'-methylenebisacrylamide; PDVB: polydivinylbenzene; PMBA: poly(N,N'-methylenebisacrylamide); NMR: nuclear magnetic resonance; CD: circular dichroism; TCP: tetrakis(4-carboxyphenyl)porphyrin.

of PCL after 3 min, while it took over 50 min without SiO_2 [Figure 8A and B]^[49]. More importantly, the twist handedness of PCL lamellae is controlled by the chirality of SiO_2 . When rotating the samples around the axis from the observer toward the microscope, the extinction rings moving upward along the rotation axis indicate the right-handed twist, while downward movement represents the left-handed twist [Figure 8C]. Without SiO_2 , the ratio between left- and right-handed twist (L:R) is close to 1:1 [Figure 8D]. However, favorable handedness of twisting is observed in the presence of chiral SiO_2 , with right-handed twists being more common than left-handed ones (L:R \approx 1:2) with D- SiO_2 , while left-handed ones increased obviously (L:R \approx 2:1) with L- SiO_2 . It seems that the alignment of the chain folds of PCL may be influenced by chiral silica and thus a given handedness of twist is preferred.

CIRCULARLY POLARIZED LUMINESCENCE FROM SiO_2 -CONTAINING NANOMATERIALS

CPL is another chiroptical phenomenon and is referred to as the difference between left-handed circularly polarized light (LCP) and right-handed circularly polarized light (RCP) in the emission from a chiral luminescent system. A CPL spectrum is collected by measuring the value of " $I_L - I_R$ " (where I_L and I_R is the intensity of LCP and RCP, respectively) at a given emission wavelength. A dissymmetry factor of g_{lum} is used to assess the differences between LCP and RCP in the total emission: $g_{\text{lum}} = 2 \times (I_L - I_R)/(I_L + I_R)$. Different from CD spectra associated ground states, CPL is related to the excitation states and provides an important spectroscopic method for chirality analysis. Moreover, CPL is useful in many areas including circularly polarized light sources, optical storage, sensing and anti-counterfeiting^[50]. A CPL active system contains two

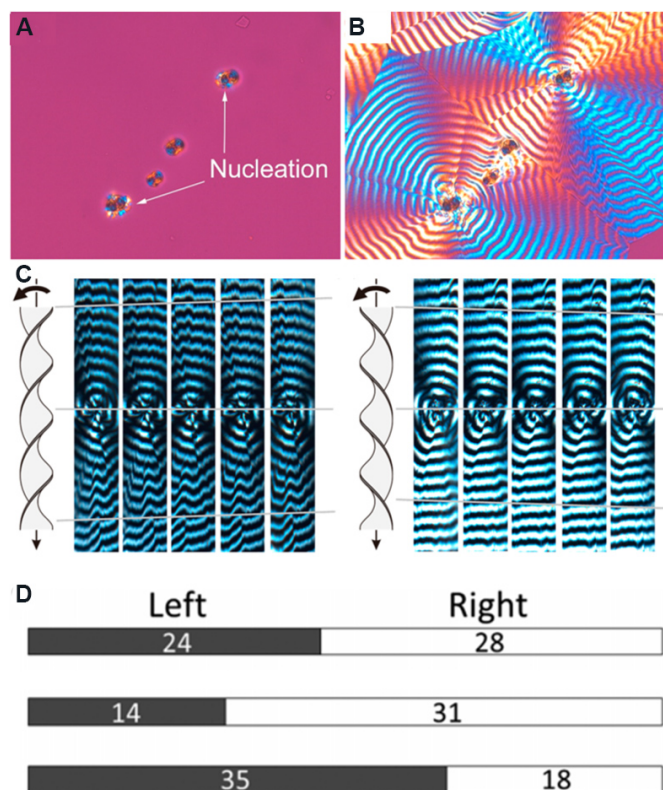


Figure 8. Polarized optical micrographs of PCL spherulites in PCL/PVB blends showing (A) nucleation of PCL on the silica particles and (B) PCL spherulites. (C) Upward (left) and downward (right) displacement of the extinction bands of PCL spherulites (the vertical and round arrows indicating the rotation axis and direction, respectively). (D) Fractions of left- and right-handed twists without silica (top), with D-SiO₂ (middle) and L-SiO₂ (bottom). This figure is used with permission from the American Chemical Society^[49]. PCL: Poly(ϵ -caprolactone); PVB: poly(vinylbutyral).

functional units: one is the luminescent part for emission and the other is the chiral one to disequilibrate LCP and RCP. As testified in the examples below, chiral SiO₂ nanofibers are good chiral sources to synthesize CD active materials, which are extended to design CPL active systems by incorporating luminescent guests.

A first example is to prepare sub-10 nm fluorescent lanthanide oxide NPs on SiO₂ nanofibers. Eu³⁺ (or Tb³⁺) ions absorbed by PEI/tart@SiO₂ are transformed into sub-10 nm crystalline Eu₂O₃ (or Tb₂O₃) NPs after calcination at 900 °C [Figure 9A]^[51]. Around the characteristic emission bands of lanthanide ions (615 nm for Eu₂O₃ and 545 nm for Tb₂O₃), the positive CPL signals (i.e., $I_L > I_R$) of these NPs on L-SiO₂ appear, while negative signals (i.e., $I_L < I_R$) occur on D-SiO₂ [Figure 9B]. According to X-ray photoelectron spectroscopy characterization, it is probable that Eu-O (or Tb-O) clusters are asymmetrically distorted in the chiral microenvironment of SiO₂ nanoreactors.

Other luminophores can also become CPL active once they are embedded within these SiO₂ nanofibers^[52]. For instance, amine group-modified SiO₂ (1°P-SiO₂, Figure 6A) is used to prepare perovskite (MAPbBr₃) NPs with CPL signals of ~520 nm [Figure 9C and D]. Moreover, various fluorescent carboxylic molecules (5,10,15,20-TCPP, 1-pyrenecarboxyl acid and fluorescein) are easily absorbed by the amine groups on SiO₂ and therefore show CPL signals at their emission wavelengths with g_{lum} of $2-5 \times 10^{-3}$ [Figure 9E]. Aggregation-induced emission (AIE) is a fascinating luminescent process and AIE-based CPL is also present in chiral SiO₂ using the typical AIE luminogens of tetraphenylethane (TPE) as a model. TPE

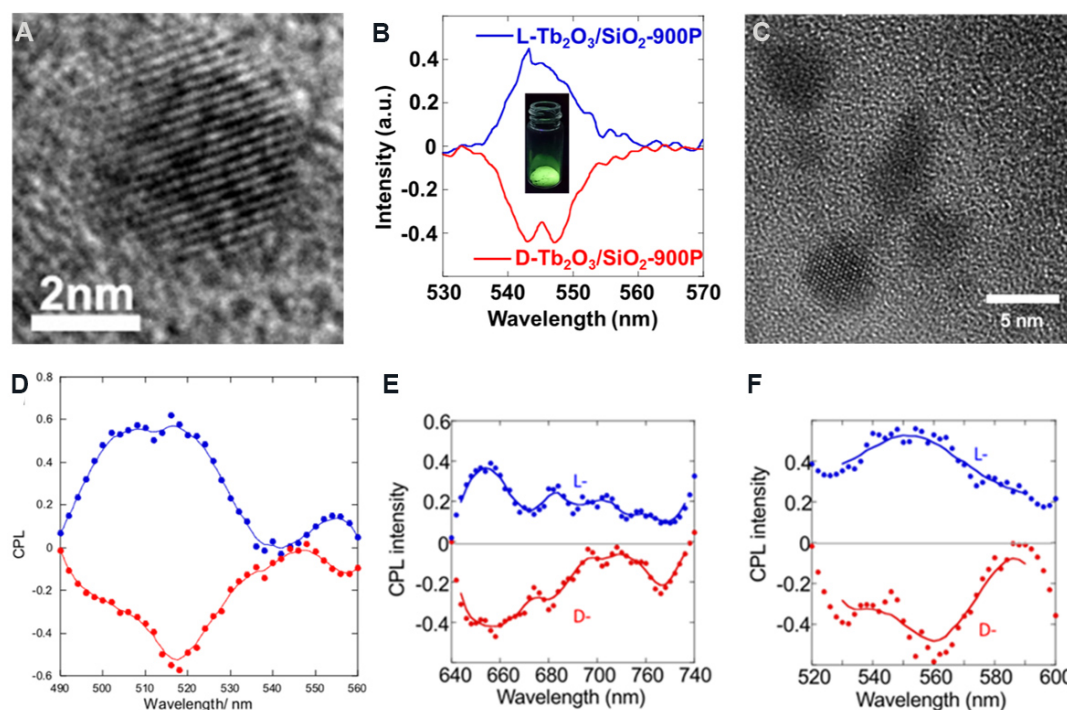


Figure 9. (A) TEM image of Eu_2O_3 NPs in $\text{D-Eu}_2\text{O}_3/\text{SiO}_2$. (B) CPL spectra of $\text{SiO}_2/\text{Tb}_2\text{O}_3$ (insert, emission photograph of $\text{SiO}_2/\text{Tb}_2\text{O}_3$ powders in dark). These figures are used with permission from John Wiley and Sons^[51]. (C) TEM image of MAPbBr_3 NPs from $\text{MAPbBr}_3@1^\circ\text{P-SiO}_2$. (D-F) CPL spectra of (D) $\text{MAPbBr}_3@1^\circ\text{P-SiO}_2$, (E) $\text{TCPP}@1^\circ\text{P-SiO}_2$ and (F) $\text{TPE}@Ph\text{-SiO}_2$. These figures are used with permission from John Wiley and Sons^[52]. TEM: Transmission electron microscopy; NPs: nanoparticles; CPL: circularly polarized luminescence; TCPP: tetrakis(4-carboxyphenyl)porphyrin.

molecules are enriched in proximity to SiO_2 nanofibers modified with phenyl groups and thus display CPL activity at ~ 476 nm in their aggregated state [Figure 9F].

In some recent works, Liu *et al.*^[53] and Harada *et al.*^[54] also used helical silica nanomaterials [Figure 1B] as chiral hosts to synthesize lanthanide ion- and perovskite-containing CPL systems. The related CPL signals and values of g_{lum} obtained using helical SiO_2 are comparable to those using SiO_2 nanofibers. However, an additional assembly process of perovskite NPs along helical SiO_2 to form a helical pattern is needed for the generation of CPL signals^[53]. In contrast, CPL relies on the molecular-scale chirality transfer from SiO_2 nanofibers and shows a weak correlation with the nano/micromorphologies at higher length levels, which seems adaptable to many applications.

RAMAN ENANTIOSELECTIVE RECOGNITION ASSISTED BY CHIRAL SiO_2 -DERIVED NANOMATERIALS

Raman spectroscopy is useful for molecule identification and has high species specificity and sensitivity to molecular interactions. Unfortunately, normal Raman spectroscopy is unable to distinguish a pair of enantiomers. Many chiral nanomaterials show different interactions toward a pair of enantiomers; however, these differences are usually too weak to detect. When a pair of enantiomers interact with a given chiral surface, they may generate differential Raman scattering signals^[55,56]. Thus, it is possible to develop novel chiral recognition methods by the combination between Raman spectroscopy and chiral SiO_2 -based nanomaterials.

To improve the affinity between SiO₂ nanofibers and the target chiral molecules, D- (or L-)SiO₂ is firstly modified by polydopamine (PDA), which is known to be a versatile surface modifier, to obtain D- (or L-) SiO₂/PDA [Figure 10A]^[57]. The PDA layers on SiO₂ become chiroptically active in the CD spectra. The chiral recognition performance of SiO₂/PDA has been checked using D- and L-cysteine (Cys) enantiomers as the models. After mixing D-SiO₂/PDA with D-Cys (or L-Cys), the as-formed “D-SiO₂/PDA & D-Cys” (or “D-SiO₂/PDA & L-Cys”) mixture is subjected to Raman spectroscopy. As shown in the Raman spectra [Figure 10B], the Raman signals for “D-SiO₂/PDA & D-Cys” and “D-SiO₂/PDA & L-Cys” share the same Raman shifts but show different signal intensities. Typically, the signal from D-Cys at 498 cm⁻¹ (denoted as I₄₉₈) is ~2.8 times as strong as that from L-Cys [Figure 10C]. However, when L-SiO₂/PDA is used, the I₄₉₈ from L-Cys is ~2.2 times that of D-Cys. As a control experiment, racemic DL-SiO₂ was used to synthesize DL-SiO₂/PDA. However, the Raman signals from D-Cys are almost the same as those from L-Cys when mixed with DL-SiO₂/PDA, indicating a poor chiral discrimination. Similar enantioselective results are found when other enantiomers are used (e.g., cystine, phenylalanine and tryptophan).

Furthermore, Ag NPs synthesized on SiO₂/PDA were isolated after the removal of SiO₂ by a HF (aq) solution [Figure 10A] to obtain PDA/Ag^[58]. Interestingly, D- (or L-) PDA/Ag also exhibits chiral discrimination toward tyrosine (Tyr) enantiomers [Figure 10D and E]. In the presence of D-PDA/Ag, the characteristic Raman signal intensity at 828 cm⁻¹ (I₈₂₈) from D-Tyr is over three times stronger than that from L-Tyr, while the I₈₂₈ from D-Tyr is weaker than that from L-Tyr when mixed with L-PDA/Ag. In a control experiment, however, the differences in Raman signals are very small when performed on achiral PDA/Ag (A-PDA/Ag) and racemic DL-PDA/Ag.

Moreover, chiral Au NPs [Figure 3] liberated from SiO₂ nanofibers are also capable of enantioselective discrimination between cystine enantiomers with similar Raman scattering differences^[59]. These results in the cases of PDA/Ag and Au NPs imply that chirality transfer has occurred from SiO₂ to PDA/Ag and Au NPs. The Raman signals are dependent upon the local concentrations, configurations and orientations of target molecules, which can be regulated by the molecular-scale chiral structures on these SiO₂-derived nanomaterials. As a consequence, enantioselective Raman scattering signals are collected for chirality recognition. In addition, the Raman scattering on plasmonic Au and Ag NPs is also controlled by the local electromagnetic field resulted from the collective excitation of the electron gas near the metallic surface^[60]. During chiral interactions, electron redistribution is possible to induce the change in electromagnetic field and Raman scattering^[61]. Although more research is required to reveal the underlying mechanism, it is believed that Raman spectroscopy will find more applications in chirality analysis and provide us with new insights on “matter-matter” and “matter-light” chiral interactions.

CONCLUSION AND OUTLOOK

If we perceive SiO₂ as a kind of polymer with repeating monomers of SiO₄ tetrahedra, it is easy to understand its molecular-scale chirality by borrowing the familiar concept of molecular chirality in organic and polymer chemistry. In principle, by adjusting the lengths of Si-O bonds and the angles of -O-Si-O-bonds, asymmetric SiO₄ tetrahedra are allowed to exist in a left-handed geometry and its counter-enantiomeric form of a right-handed one. The asymmetry of SiO₄ units brings about chiral structures of SiO₂ on a larger scale. With this in mind, an efficient synthesis strategy for enantiomerically enriched SiO₂ has been established with handedness control on the early stage of SiO₂ sol formation by chiral PEI/tart templates. Although the exact chiral structural information is not currently clear, the chiral properties of SiO₂ close to the molecular scale have been manifested with significant evidence. Moreover, these SiO₂ structures can activate the chirality of various molecules, nanomaterials and even optical phenomena, which are supposed to be achiral traditionally. In this regard, asymmetric silica is a versatile messenger for chirality

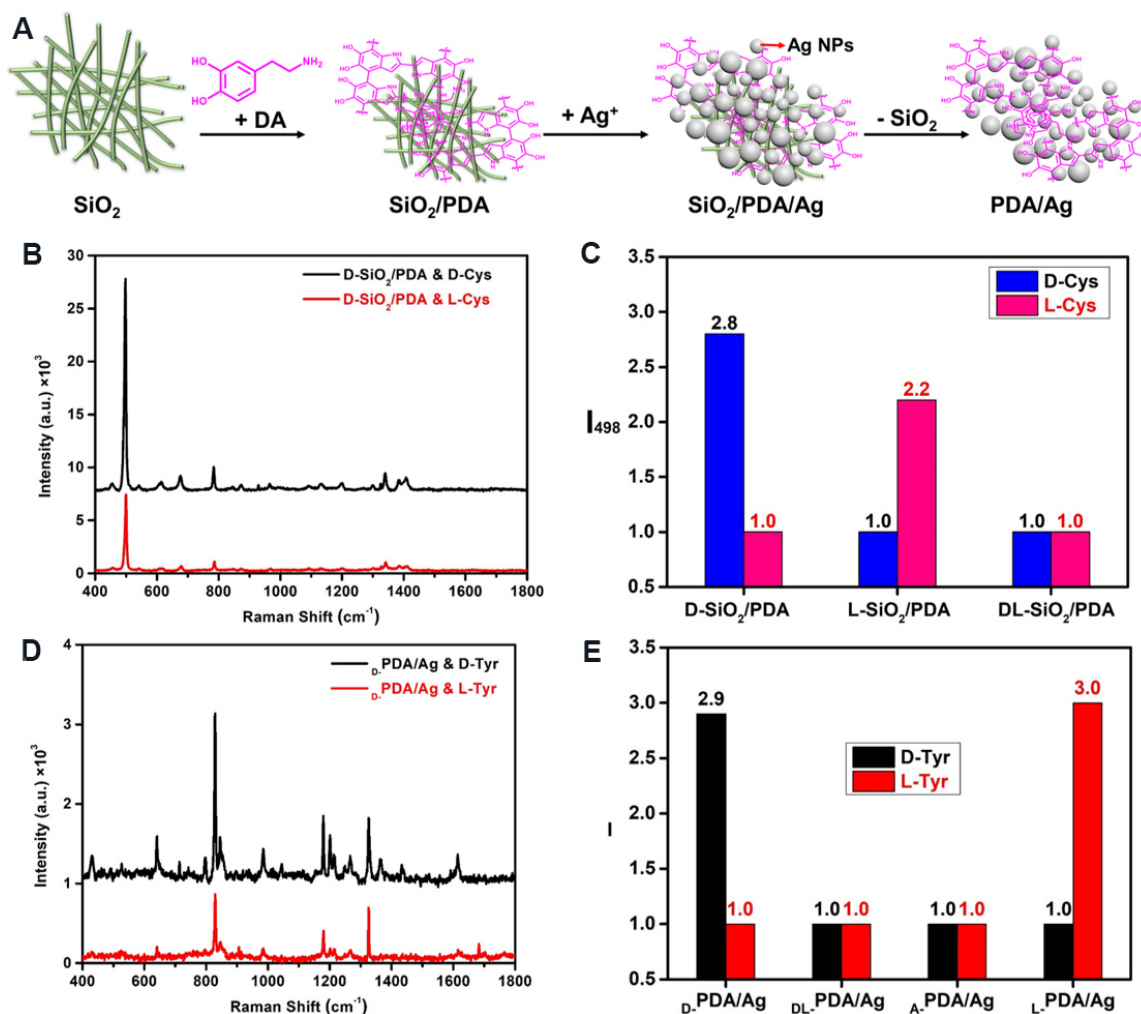


Figure 10. (A) Schematic description of synthesis of SiO₂/PDA and PDA/Ag. This figure is used with permission from the American Chemical Society^[58]. (B) Raman spectra for “D-SiO₂/PDA & D-Cys” and “D-SiO₂/PDA & L-Cys”. (C) Relative values of I_{498} for cysteine after mixing with D-, L- and DL-SiO₂/PDA; D-SiO₂/PDA. This figure is used with permission from the American Chemical Society^[57]. (D) Raman spectra for “D-PDA/Ag & D-Tyr” and “D-PDA/Ag & L-Tyr”. (E) Relative values of I_{828} for tyrosine after mixing with D-, L-, A- and DL-PDA/Ag. This figure is used with permission from the American Chemical Society^[58]. NPs: Nanoparticles; PDA: polydopamine.

communication among organics, inorganics and light. Considering the abundance and extensive use of silica, a broad chiral world on the molecular scale is anticipated, which may offer chances to unveil homochirality in the origin of life and develop innovative techniques.

Although we have established a method of preparing SiO₂ nanofibers with molecular-level chiral structures and demonstrated their applications in the synthesis of cross-linked polymers and inorganic nanoparticles, CPL and Raman scattering-based enantioselective recognition, the following aspects are worthy of study to understand the chiral features of SiO₂ in the future:

(1) Development of new synthesis methods of chiral SiO₂, which is significant to provide more models to probe the chiral properties of SiO₂.

(2) Detailed structural analysis of SiO₂ to reveal the parameters of Si-O bonds, which requires advanced characterization techniques (e.g., synchrotron radiation analysis and neutron diffraction) and simulation methods.

(3) Exploration of potential applications of chiral SiO₂ in various areas, including: (I) asymmetric synthesis of small chiral molecules or simulated prebiotic chemical processes triggered by chiral SiO₂; (II) chiral separation by using chiral SiO₂ as the stationary phase in chromatography; (III) construction of novel chiral silicate materials by virtue of the high thermal stability and chirality transfer ability of SiO₂; (IV) the enantioselective interactions between SiO₂ and bio-/drug molecules to improve therapeutic effects; and (V) optical phenomena (e.g., absorption, luminescence and scattering)-based applications with chiral responses for sensing, 3D displays, information storage and anti-counterfeiting.

(4) Clarification of the mechanism of chirality transfer during the formation of chiral SiO₂ and other processes regulated by SiO₂.

DECLARATIONS

Authors' contributions

Prepared and corrected the manuscript: Liu X, Jin RH

Availability of data and materials

Not applicable.

Financial support and sponsorship

The research was supported in part by the JSPS KAKENHI, grant number: JP16H06515 (Coordination Asymmetry) and by the JSPS KAKEHI Grantin-Aid for Scientific Research (B), 19H02767.

Conflicts of interest

Both authors declared that there are no conflicts of interest.

Ethical approval and consent to participate

Not applicable.

Consent for publication

Not applicable.

Copyright

© The Author(s) 2021.

REFERENCES

1. Gal J. Pasteur and the art of chirality. *Nat Chem* 2017;9:604-5. [DOI](#) [PubMed](#)
2. Dyakin VV, Lucas J, Dyakina-fagnano NV, Posner EV; The Nathan S. Kline Institute for Psychiatric Research. The chain of chirality transfer as determinant of brain functional laterality. Breaking the chirality silence: search for new generation of biomarkers; relevance to neurodegenerative diseases, cognitive psychology, and nutrition science. *Neurology and Neuroscience Research* 2017;1:2. [DOI](#)
3. Zhao X, Zang SQ, Chen X. Stereospecific interactions between chiral inorganic nanomaterials and biological systems. *Chem Soc Rev* 2020;49:2481-503. [DOI](#) [PubMed](#)
4. Shao Y, Yang G, Lin J, et al. Shining light on chiral inorganic nanomaterials for biological issues. *Theranostics* 2021;11:9262-95. [DOI](#) [PubMed](#) [PMC](#)
5. Liu J, Yang L, Qin P, Zhang S, Yung KKL, Huang Z. Recent advances in inorganic chiral nanomaterials. *Adv Mater* 2021;33:e2005506. [DOI](#) [PubMed](#)
6. Ni B, Cölfen H. Chirality communications between inorganic and organic compounds. *SmartMat* 2021;2:17-32. [DOI](#)
7. Lowry TM. Optical rotatory dispersion: a tribute to the memory of biot (1774-1862). *Nature* 1926;117:271-5. [DOI](#)
8. Jung JH, Ono Y, Hanabusa K, Shinkai S. Creation of both right-handed and left-handed silica structures by sol-gel transcription of

- organogel fibers comprised of chiral diaminocyclohexane derivatives. *J Am Chem Soc* 2000;122:5008-9. DOI
9. Che S, Liu Z, Ohsuna T, Sakamoto K, Terasaki O, Tatsumi T. Synthesis and characterization of chiral mesoporous silica. *Nature* 2004;429:281-4. DOI PubMed
 10. Qiu H, Wang S, Zhang W, et al. Steric and temperature control of enantiopurity of chiral mesoporous silica. *J Phys Chem C* 2008;112:1871-7. DOI
 11. Yang Y, Suzuki M, Owa S, Shirai H, Hanabusa K. Control of mesoporous silica nanostructures and pore-architectures using a thickener and a gelator. *J Am Chem Soc* 2007;129:581-7. DOI PubMed
 12. Shopsowitz KE, Qi H, Hamad WY, MacLachlan MJ. Free-standing mesoporous silica films with tunable chiral nematic structures. *Nature* 2010;468:422-5. DOI PubMed
 13. Okazaki Y, Cheng J, Dedovets D, et al. Chiral colloids: homogeneous suspension of individualized SiO₂ helical and twisted nanoribbons. *ACS Nano* 2014;8:6863-72. DOI PubMed
 14. Shopsowitz KE, Hamad WY, MacLachlan MJ. Chiral nematic mesoporous carbon derived from nanocrystalline cellulose. *Angew Chem Int Ed Engl* 2011;50:10991-5. DOI PubMed
 15. Fireman-shoresh S, Marx S, Avnir D. Enantioselective sol-gel materials obtained by either doping or imprinting with a chiral surfactant. *Adv Mater* 2007;19:2145-50. DOI PubMed
 16. Levi G, Scolnik Y, Mastai Y. Imprinting chirality in silica nanotubes by N-stearoyl-serine template. *ACS Appl Mater Interfaces* 2016;8:23356-61. DOI PubMed
 17. Qiu H, Che S. Chiral mesoporous silica: chiral construction and imprinting via cooperative self-assembly of amphiphiles and silica precursors. *Chem Soc Rev* 2011;40:1259-68. DOI PubMed
 18. Marx S, Avnir D. The induction of chirality in sol-gel materials. *Acc Chem Res* 2007;40:768-76. DOI PubMed
 19. Kawasaki T, Araki Y, Hatase K, et al. Helical mesoporous silica as an inorganic heterogeneous chiral trigger for asymmetric autocatalysis with amplification of enantiomeric excess. *Chem Commun (Camb)* 2015;51:8742-4. DOI PubMed
 20. Faridi A, Sun Y, Okazaki Y, et al. Mitigating human IAPP amyloidogenesis in vivo with chiral silica nanoribbons. *Small* 2018;14:e1802825. DOI PubMed PMC
 21. Huang Y, Vidal X, Garcia-Bennett AE. Chiral resolution using supramolecular-templated mesostructured materials. *Angew Chem Int Ed Engl* 2019;58:10859-62. DOI PubMed
 22. Gou K, Wang Y, Xie L, et al. Synthesis, structural properties, biosafety and applications of chiral mesoporous silica nanostructures. *Chem Eng J* 2021;421:127862. DOI
 23. Salh R. Defect related luminescence in silicon dioxide network: a review. In: Basu S, editor. Crystalline silicon. London: IntechOpen Limited; 2011. p. 135-72. DOI
 24. Tanaka Y, Takeuchi T, Lovesey SW, et al. Right handed or left handed? *Phys Rev Lett* 2008;100:145502. DOI PubMed
 25. Will G, Bellotto M, Parrish W, Hart M. Crystal structures of quartz and magnesium germanate by profile analysis of synchrotron-radiation high-resolution powder data. *J Appl Crystallogr* 1988;21:182-91. DOI
 26. Yogeve-einot D, Avnir D. Quantitative symmetry and chirality of the molecular building blocks of quartz. *Chem Mater* 2003;15:464-72. DOI
 27. Dryzun C, Mastai Y, Shvalb A, Avnir D. Chiral silicate zeolites. *J Mater Chem* 2009;19:2062. DOI
 28. Belton DJ, Deschaume O, Perry CC. An overview of the fundamentals of the chemistry of silica with relevance to biosilicification and technological advances. *FEBS J* 2012;279:1710-20. DOI PubMed PMC
 29. Shimizu K, Cha J, Stucky GD, Morse DE. Silicatein alpha: cathepsin L-like protein in sponge biosilica. *Proc Natl Acad Sci U S A* 1998;95:6234-8. DOI PubMed PMC
 30. Abdelhamid MAA, Pack SP. Biomimetic and bioinspired silicifications: recent advances for biomaterial design and applications. *Acta Biomater* 2021;120:38-56. DOI PubMed
 31. Jin RH, Yuan JJ. Synthesis of poly(ethyleneimine)-silica hybrid particles with complex shapes and hierarchical structures. *Chem Commun (Camb)* 2005:1399-401. DOI PubMed
 32. Yuan J, Jin R. Multiply shaped silica mediated by aggregates of linear poly(ethyleneimine). *Adv Mater* 2005;17:885-8. DOI
 33. Yuan J, Zhu P, Fukazawa N, Jin R. Synthesis of nanofiber-based silica networks mediated by organized poly(ethylene imine): structure, properties, and mechanism. *Adv Funct Mater* 2006;16:2205-12. DOI
 34. Matsukizono H, Jin RH. High-temperature-resistant chiral silica generated on chiral crystalline templates at neutral pH and ambient conditions. *Angew Chem Int Ed Engl* 2012;51:5862-5. DOI PubMed
 35. Matsukizono H, Murada H, Jin RH. Nanosheet-stacked chiral silica transcribed from metal ion- and pH-tuned supramolecular crystalline complexes of polyamine-D-glucarate. *Chemistry* 2014;20:1134-45. DOI PubMed
 36. Liu XL, Tsunega S, Jin RH. Self-directing chiral information in solid-solid transformation: unusual chiral-transfer without racemization from amorphous silica to crystalline silicon. *Nanoscale Horiz* 2017;2:147-55. DOI PubMed
 37. Wallace AF, DeYoreo JJ, Dove PM. Kinetics of silica nucleation on carboxyl- and amine-terminated surfaces: insights for biomineralization. *J Am Chem Soc* 2009;131:5244-50. DOI PubMed
 38. Jin RH. Understanding silica from the viewpoint of asymmetry. *Chemistry* 2019;25:6270-83. DOI PubMed
 39. Xie J, Duan Y, Che S. Chirality of metal nanoparticles in chiral mesoporous silica. *Adv Funct Mater* 2012;22:3784-92. DOI
 40. Okazaki Y, Ryu N, Buffeteau T, et al. Induced circular dichroism of monoatomic anions: silica-assisted the transfer of chiral environment from molecular assembled nanohelices to halide ions. *Chem Commun (Camb)* 2018;54:10244-7. DOI PubMed
 41. Tsunega S, Tanabe T, Jin R. Unusual chirality transfer from silica to metallic nanoparticles with formation of distorted atomic array in crystal lattice structure. *Nanoscale Adv* 2019;1:581-91. DOI

42. Wei X, Liu J, Xia GJ, et al. Enantioselective photoinduced cyclodimerization of a prochiral anthracene derivative adsorbed on helical metal nanostructures. *Nat Chem* 2020;12:551-9. DOI PubMed
43. Price AJ, Johnson ER. Theoretical investigation of amino-acid adsorption on hydroxylated quartz surfaces: dispersion can determine enantioselectivity. *Phys Chem Chem Phys* 2020;22:16571-8. DOI PubMed
44. Kotopoulou E, Lopez-Haro M, Calvino Gamez JJ, Garcia-Ruiz JM. Nanoscale anatomy of iron-silica self-organized membranes: implications for prebiotic chemistry. *Angew Chem Int Ed Engl* 2021;60:1396-402. DOI PubMed PMC
45. Liu XL, Moriyama K, Gao YF, Jin RH. Polycondensation and carbonization of phenolic resin on structured nano/chiral silicas: reactions, morphologies and properties. *J Mater Chem B* 2016;4:626-34. DOI PubMed
46. Liu X, Tsunega S, Ito T, et al. Double chiral hybrid materials: formation of chiral phenolic resins on polyamine-associated chiral silica. *Chem Lett* 2017;46:1518-21. DOI
47. Tsunega S, Kongpitak P, Jin R. Chiroptical phenolic resins grown on chiral silica-bonded amine residues. *Polym Chem* 2019;10:3535-46. DOI
48. Tsunega S, Jin R. Chiroptical cross-linked polymers grown via radical polymerization around chiral nanosilica. *Macromol Chem Phys* 2021;222:2000436. DOI
49. Ikehara T, Kataoka T, Inutsuka M, Jin R. Chiral nucleating agents affecting the handedness of lamellar twist in the banded spherulites in poly(ϵ -caprolactone)/poly(vinyl butyral) blends. *ACS Macro Lett* 2019;8:871-4. DOI
50. Sang Y, Han J, Zhao T, Duan P, Liu M. Circularly polarized luminescence in nanoassemblies: generation, amplification, and application. *Adv Mater* 2020;32:e1900110. DOI PubMed
51. Sugimoto M, Liu XL, Tsunega S, et al. Circularly polarized luminescence from inorganic materials: encapsulating guest lanthanide oxides in chiral silica hosts. *Chemistry* 2018;24:6519-24. DOI PubMed
52. Tsunega S, Jin RH, Nakashima T, Kawai T. Transfer of chiral information from silica hosts to achiral luminescent guests: a simple approach to accessing circularly polarized luminescent systems. *Chempluschem* 2020;85:619-26. DOI PubMed
53. Liu P, Chen W, Okazaki Y, et al. Optically active perovskite CsPbBr₃ nanocrystals helically arranged on inorganic silica nanohelices. *Nano Lett* 2020;20:8453-60. DOI PubMed
54. Harada T, Yanagita H, Ryu N, et al. Lanthanide ion-doped silica nanohelix: a helical inorganic network acts as a chiral source for metal ions. *Chem Commun (Camb)* 2021;57:4392-5. DOI PubMed
55. Wang Y, Zhao X, Yu Z, Xu Z, Zhao B, Ozaki Y. A chiral-label-free SERS strategy for the synchronous chiral discrimination and identification of small aromatic molecules. *Angew Chem Int Ed Engl* 2020;59:19079-86. DOI PubMed
56. Liu Z, Ai J, Kumar P, et al. Enantiomeric discrimination by surface-enhanced raman scattering-chiral anisotropy of chiral nanostructured gold films. *Angew Chem Int Ed Engl* 2020;59:15226-31. DOI PubMed
57. Kong H, Sun X, Yang L, Liu X, Yang H, Jin RH. Chirality detection by raman spectroscopy: the case of enantioselective interactions between amino acids and polymer-modified chiral silica. *Anal Chem* 2020;92:14292-6. DOI PubMed
58. Kong H, Sun X, Yang L, Liu X, Yang H, Jin RH. Polydopamine/silver substrates stemmed from chiral silica for SERS differentiation of amino acid enantiomers. *ACS Appl Mater Interfaces* 2020;12:29868-75. DOI PubMed
59. Sun X, Kong H, Zhou Q, et al. Chiral plasmonic nanoparticle assisted raman enantioselective recognition. *Anal Chem* 2020;92:8015-20. DOI PubMed
60. Pérez-Jiménez AI, Lyu D, Lu Z, Liu G, Ren B. Surface-enhanced Raman spectroscopy: benefits, trade-offs and future developments. *Chem Sci* 2020;11:4563-77. DOI PubMed PMC
61. Kumar A, Capua E, Kesharwani MK, et al. Chirality-induced spin polarization places symmetry constraints on biomolecular interactions. *Proc Natl Acad Sci U S A* 2017;114:2474-8. DOI PubMed PMC